Single-cell bacterial electrophysiology reveals mechanisms of stress-induced damage

Single-cell bacterial electrophysiology reveals mechanisms of stress induced damage

Ekaterina Krasnopeeva[1], Chien-Jung Lo[2], and Teuta Pilizota[1]

[1]**Centre for Synthetic and Systems Biology, Institute of Cell Biology, School of Biological Sciences, University of Edinburgh, Alexander Crum Brown Road, EH9 3FF, Edinburgh, UK**
[2]**Department of Physics and Graduate Institute of Biophysics, National Central University, Jhongli, Taiwan 32001, ROC**

ABSTRACT

Electrochemical gradient of protons, or proton motive force (PMF), is at the basis of bacterial energetics. It powers vital cellular processes and defines the physiological state of the cell. Here we use an electric circuit analogy of an *Escherichia coli* cell to mathematically describe the relationship between bacterial PMF, electric properties of the cell membrane and catabolism. We combine the analogy with the use of bacterial flagellar motor as a single-cell "voltmeter" to measure cellular PMF in varied and dynamic external environments, for example, under different stresses. We find that butanol acts as an ionophore, and functionally characterise membrane damage caused by the light of shorter wavelengths. Our approach coalesces non-invasive and fast single-cell voltmeter with a well-defined mathematical framework to enable quantitative bacterial electrophysiology.

Keywords: bacterial energetics, proton motive force, bacterial membrane damage, single-cell measurements, bacterial physiology, indole, butanol, photodamage

INTRODUCTION

To stay alive bacteria, like other cells, maintain adequate supplies of free energy, and under various external stresses attempt to stay viable by distributing it to processes essential for coping with the challenge, while simultaneously maintaining core cellular functions. The two main sources of free energy in living cells are adenosine triphosphate (ATP) molecule and proton motive force (PMF). The ATP molecule is the energy "currency" of living organisms used for biosynthesis and transport. The PMF is a direct consequence of the activity of the electron transport chain or substrate level phosphorylation, and serves as the energy source driving numerous cellular processes: ATP production, motility and active membrane transport. The two are interlinked, ordinarily PMF is used to synthesise ATP, but ATP can drive the production of PMF as well (1).

As early as 1791 Luigi Galvani proposed that life processes generate electricity (2; 3). However, it took more than a century for Hugo Fricke to measure the capacitance of biological membrane (4) and for Peter Mitchell to explain that PMF is an electrochemical gradient of protons across the membrane that powers the production of ATP (5). PMF consists of the two components: pH difference between cytoplasm and the external environment ($\Delta pH = pH_{in} - pH_{out}$), and the electrical potential across the membrane (V_m, we note that the build up of charge occurs at $\sim$ nm-thin layer close to the biological membrane (6)).

$$PMF = V_m - \frac{2.303kT}{e}\Delta pH \tag{1}$$

where k is the Boltzmann constant, T is the temperature and e is the elementary charge.

Since life generates electricity used to power its processes and cell membrane acts as a capacitor, it is reasonable to represent the rest of the cell components with an electrical circuit analogy (7; 8), Fig. 1A. Then,

proton fluxes are currents, oxidative or substrate-level phosphorylation can be considered as an imperfect battery with non-zero internal resistance, and the membrane resistance and capacitance are connected in parallel. Membrane voltage in this analogy is equivalent to the drop of potential on the external resistance. Cytoplasmic pH of *Escherichia coli* is kept within the pH 7.2-7.8 range (9; 10; 11). Thus, a cell placed in an external environment whose pH matches its internal pH, has negligible contribution of the pH difference to the total PMF, and V_m in the circuit becomes equivalent to the PMF (see equation (1)).

The circuit analogy in Fig. 1A gives a mathematical framework that helps us understand cellular free energy maintenance in a range of different conditions. For example, we can predict changes in V_m when circuit parameters change: a battery depends on the available carbon source, and internal resistance R_i increases in presence of electron transport chain inhibitors (such as sodium azide (12)). Furthermore, if we could measure V_m with an equivalent of a "voltmeter" we could predict the mechanism and dynamics of the damage as the cells are exposed to various external stresses, as well as obtain functional dependence between affected circuit parameters and the amplitude of the stress.

Here we report the use of bacterial flagellar motor (BFM) as such a "voltmeter". BFM is a nano-machine that enables bacterial swimming (13) via PMF powered rotation (14; 15; 16; 17). The motor sturucture and function have been a topic of active reserach for several decades (13), however BFM has not yet been applied as an indicator. Because the motor speed varies linearly with PMF (17; 18), we reasoned that it can be used as a robust "PMF-meter" that offers high temporal resolution. When combined with an "electrical circuit interpretation" of the cell, such high-precision, non-invasive, PMF (V_m) measurements become a powerful new approach needed for quantitative bacterial electrophysiology. We demonstrate it by revealing mechanisms of damage caused by chosen stresses; we confirm the behaviour of a known ionophore (indole) (19), discover that butanol is an ionophore, and quantitatively describe the nature of damage caused by the light of shorter wavelengths.

MATERIALS AND METHODS

E. coli strains

E. coli EK07 strain is constructed as described in *Supplementary Materials*, which includes a figure with plasmid maps and a table with the primers. Highly motile *E. coli* strain MG1655 with an insertion sequence element in the *flhD* operon (20) is modified to have *fliC* gene replaced by $fliC^{sticky}$ (21), which produces flagellar filaments that stick to glass or polystyrene surfaces. Additionally, *pHluorin* (22; 23) gene under strong constitutive *Vibrio harveyi* cytochrome C oxidase promoter (24) is placed onto *att*Tn7 site of the chromosome. All the chromosomal alterations are generated using plasmid mediated gene replacement technique (25).

E. coli growth and media

EK07 cells are grown in Lysogeny broth (LB: 10 g tryptone, 5 g yeast extract, 10 g NaCl per 1 L). The overnight culture (OD=5.5) frozen and stored at -80°C in presence of 20% glycerol is thawed and diluted in a fresh LB to the OD $\approx$ 0.003 (1x1000 dilution from the overnight culture) and grown at 37°C with shaking (220 rpm) to OD=2.0 (Spectronic 200E Spectrophotometer, Thermo Scientific, UK). The OD at harvest is chosen to maximise the number of motors per cell (26) and, thus, increase the yield of the single motor experiments. Growth curves of the EK07 and the parent MG1655 strain are given in SI Fig. 1. After growth cells are washed (3 times by centrifugation at 8000 g for 2 min) into MM9 (aqueous solution of 50 mM Na_2HPO_4, 25 mM NaH_2PO_4, 8.5 mM NaCl and 18.7 mM NH_4Cl with added 0.1 mM $CaCl_2$, 1 mM KCl, 2 mM $MgSO_4$ and 0.3% D-glucose) adjusted to pH=7.5 or PBS (aqueous solution of 154 mM NaCl, 5 mM Na_2HPO_4 and 1.5 mM KH_2PO_4) adjusted to pH=7.5. Indole treatment is performed in MM9 and butanol and photodamage experiments in MM9 and PBS.

Microscope slides preparation

To shorten flagella, cells are "sheared" as described previously (27; 28) and washed as above. For butanol and indole treatment tunnel-slides are prepared as before ((28), see also SI Fig. 2A). For photodamage experiments flow-cells are manufactured by drilling (AcerDent, UK) two 1.8 mm holes on opposite ends of the microscope slide and attaching Tygon® Microbore tubing (Saint Gobain Performance Plastics, France). The flow-cell is then created by attaching gene frame (Fisher Scientific Ltd, USA) to the slide and covering it with a cover glass (SI Fig. 2B). Surface of the cover slide is coated with 0.1% poly-L-lysine (PLL) by flushing PLL through the flow-cell/tunnel-slide for ∼10 s followed by washing it out with the excessive volume of growth medium. The surface coating protocol we are using does not result in observable growth rate, nor internal pH changes when compared to growth on agarose pad in the same medium (29). Sheared and washed cells are then loaded into the flow-cell/tunnel-slide and incubated for 10 min to allow attachment. Excessive cells are washed out with the growth medium. Subsequently, 0.5 μm in diameter polystyrene beads (Polysciences, Inc, USA) in either PBS or MM9 are added to the flow-cell/tunnel-slide and incubated for 10 min with consequent washing out of the non-attached beads.

Microscopy and data collection

Back-focal-plane interferometry (30; 31) is performed as previously described (28). Briefly, heavily attenuated optical trap (855 nm laser) is used to detect the rotation of a polystyrene bead attached to a truncated flagellar filament (Fig. 1B). Time course of the bead rotation is recorded with the position-sensitive detector (PSD Model 2931, New Focus, USA) at 10 kHz, and a 2.5 kHz cutoff anti-aliasing filter applied before processing (Fig. 1B). Bead position (x,y) is calculated from photocurrents $I_1 - I_4$ as $(I_1 + I_2 - (I_3 + I_4))/(I_1 + I_3 + I_2 + I_4) = 2x/L$ and $(I_1 + I_3 - (I_2 + I_4))/(I_1 + I_3 + I_2 + I_4) = 2y/L$, where L is the PSD detector side length.

Fluorescent images of pH sensitive pHluorin are taken in the same custom-built microscope with iXon Ultra EMCCD camera (Andor, UK). OptoLED Dual (Cairn Research Ltd, UK) independently driving two LEDs is used for the illumination. Narrow spectrum UV LED is used for excitation at 395 nm and Neutral White LED with ET470/40x filter (Chroma Technology, USA) for 475 nm excitation. Emission is taken at 520 nm using ET525/40x filter (Chroma Technology, USA). Exposure time is fixed at 50 ms for butanol and indole treatment experiments and varies from 10 to 200 ms for photodamage experiments.

Applying stresses

1-Butanol for molecular biology, ⩾99%, and indole, analytical standard, are obtained from Sigma-Aldrich, USA. Indole is prepared from a 1 M stock solution in 98% ethanol. The highest concentration of ethanol in the indole solution used for treatment is 0.25%, which by itself does not affect motor speed significantly (see SI Fig. 3). Treatment is performed as follows: after recording the motor speed for 2 min, 20 μl of MM9 (or PBS) supplemented with a given concentration of butanol or indole is flushed into the tunnel-slide. Flush is done by placing a droplet of liquid on one, and collecting it with a piece of tissue paper on the other side of the tunnel (32). Duration of the flush is no longer than 10 s. 10 μl droplets of shocking solution are then placed on both side of the tunnel to minimise evaporation. The shock motor speed is recorded for 10 min, followed by a flush back into MM9 (or PBS) medium. Postshock speed is recorded for 5 min. The motor speed recording is uninterrupted for the duration of the experiment (total of 17 min). For pH control experiments fluorescent images are taken every 90 seconds. Control flushes with media containing no indole/butanol are shown in SI Fig. 4.

Photodamage experiments are performed as follows: using the flow-cell MM9 or PBS is constantly supplied at 10 μl/min rate with a syringe pump (Fusion 400, Chemyx Inc., USA). Cells are sequentially exposed to the light of λ=395 nm and 475 nm. Speed recording starts simultaneously with the light exposure. The camera exposure time (t_{cam}) and sampling rate are controlled with a custom written LabView program. t_{cam} are set the same for both wavelengths, however hardware adds a different delay, thus effective light exposure times are

t_{light} =225 ms+t_{cam} for 475 nm and 55 ms+t_{cam} for 395 nm. We record t_{light} and sampling rate throughout the experiment to calculate the effective light power (P_{eff}) as the total energy delivered, divided by the total length of the individual motor speed recording. Total energy delivered is estimated by measuring the illumination power in the sample plane multiplied by the total time of light exposure and divided by the illumination area. We measured the illumination area by photobleaching part of the slide and measuring the diameter of the bleached region (d $\approx$ 220 μm). Control speed traces with no light exposure are shown in SI Fig. 5.

Data analysis

A flat-top window discrete Fourier transform (window size=16384 data points with a step dt =0.01 s) is applied to x and y coordinates of bead position to obtain a time series motor speed record. This speed records we refer to as raw speed traces (Fig. 1C, 2A, 3A, 4A, SI Fig. 3, 4, 5, 8, 9). Raw traces are further processed as follows: (a) absolute values are taken, (b) values below 10 Hz are removed and 50 Hz AC frequency values disregarded, (c) remaining data points are median filtered with 201 points moving window. To calculate mean speeds we apply a 10 s moving window on the speed traces processed as above. In addition to above, photodamage traces are normalised. First, 30 s of the trace is split into 60 windows containing 50 points each. The mean of maximum values found within each window is calculated and considered the initial speed value, by which the rest of the trace is normalised. Each normalised trace is fitted with a single parameter exponential: $y = e^{-\alpha x}$. For Fig. 2D and 3D hyperbolic function fitted is $y = \frac{1}{Kx+1}$ and quadratic hyperbolic $y = \frac{1}{Kx^2+1}$, where K is a fitting parameter. All fittings are performed in Python (SciPy module, curve fit optimization) with maximum number of calls to the optimization function taken as 20 000. In the *Supplementary Materials* we give details on pHluorin image analysis and calibration (including the *in vivo* and *in vitro* calibration curves).

RESULTS

PMF measurements via flagellar motor speed can be used to analyse stress-induced damage

The electric circuit analogy (Fig. 1A) gives a mathematical framework needed to understand cellular free energy maintenance in a range of different conditions. For example, under given external stress it allows us to (a) discern the affected component of the cell represented in the circuit in Fig. 1A and (b) predict the mechanism of damage caused by the stress. To pin down the affected component of the cell we reason in the following manner. Membrane capacitance is set by the geometry of the lipid bilayer and unlikely to be altered on shorter time scales. V_c is the theoretical maximum potential a cell can generate in a given environment and from a given internalised (carbon) source. Stress can affect V_c only by damaging specific carbon transporters and, thus, it is media-dependent. Furthermore, in starvation buffer where *E. coli* uses internal carbon sources (33) V_c will not be changed by the stress. R_i defines the inefficiency of the catabolism, comprising the drop from V_c as a specific carbon source gets metabolised via a large number of catabolic enzymes. Because these enzymes are at least partially carbon source specific, the stress that targets R_i will be media-dependent. Finally, while the R_e value is growth media-dependent, the membrane targeting stresses that influence R_e will be media-independent.

Once we pin down the affected component, we employ Kirchoff's laws to express it as a function of stress-induced membrane potential change ($V_m/V_{m,0}$), which we measure using bacterial flagellar motor as a "voltmeter"(Fig. 1A). While BFM can be actively slowed down, e.g. when cell enter stationary phase (34), on shorter time scales the linearity between the motor speed (ω) and PMF allows us to use ω as a PMF indicator, and when $pH_{in} \approx pH_{out}$ as a V_m indicator as well. Here we consider only the situation where $\Delta pH \approx 0$, which we set by adjusting the external pH to known internal pH of *E. coli* (9), and in the rest of the text use PMF and V_m interchangeably. In addition, EK07 strain we constructed (see *Materials and Methods*) carries a chromosomal copy of the gene encoding pHluorin protein, which we use to check that our expectation is correct. SI Fig. 6 shows that throughout the measurements $\Delta pH \approx 0$, and that the maximum difference in pH units we

occasionally observe is maximum 0.5. This pH gradient at room temperature is equivalent to ∼30 mV of PMF, which we consider negligible as it lies within our measured standard deviation. We thus have:

$$\omega = \xi \cdot \mathrm{PMF} = \xi \cdot \mathrm{V_m} \tag{2a}$$

$$\frac{\omega}{\omega_0} = \frac{\mathrm{PMF}}{\mathrm{PMF_0}} = \frac{\mathrm{V_m}}{\mathrm{V_{m,0}}} = \mathrm{f(S,t)} \tag{2b}$$

where we assumed that ω changes as a function of stress amplitude and time f(S,t), ξ is a constant and index 0 denotes the variable value prior to stress. We measure ω using back-focal-plane interferometry (31) and a polystyrene bead attached to a short filament stub (see *Materials and Methods* and Fig. 1B) (27). An example trace of BFM speed is given in Fig. 1C. Using equation (2b) and the circuit analogy we can express each circuit component as a function of stress. To do so, we simplify the electric circuit by estimating the RC constant of the cell membrane. Capacitance and resistance of the bacterial membrane have been reported as C∼1 μF/cm^2 (35; 36) and R∼10-1000 Ohm · cm^2 (37; 19), which gives RC in the range of 10^{-5} to 10^{-3} s. Thus, the current through the capacitor (i_3) is zero prior to the stress application (when the system is in steady-state), as well as post stress application when t > 1 ms (less than our experimental resolution). Next we consider ΔG of NADH oxidation only, and compute that respiratory chain can produce $\mathrm{V_c}$ ∼-360 mV (8). Yet, physiological value of the membrane potential of respiring bacteria is approximately equal to -160 mV (38), indicating that roughly half of the membrane potential drops at the internal resistance, i.e. $\mathrm{R_{i,0}} \approx \mathrm{R_{e,0}}$. Taking the two simplifications into account we arrive to (see Fig. 1A and *Supplementary Material* for detailed deduction of equations):

$$\frac{\mathrm{V_c}}{\mathrm{V_{c,0}}} = \mathrm{f(S,t)} \tag{3a}$$

$$\frac{\mathrm{R_i}}{\mathrm{R_{i,0}}} = \frac{2}{\mathrm{f(S,t)}} - 1 \tag{3b}$$

$$\frac{\mathrm{R_e}}{\mathrm{R_{e,0}}} = \frac{\mathrm{f(S,t)}}{2 - \mathrm{f(S,t)}} \tag{3c}$$

Equations (3a) to (3c) allow us to relate changes in BFM speed, and thus cellular PMF, with the changes in the components of the electric circuit presented in Fig. 1A. To start, we included only high-level features of the cell. However, a more detailed representation of the cell in the circuit analogy is possible, e.g. external resistance may be split into parallel resistances representing lipids or specific membrane proteins.

PMF dynamics analysis confirms indole is an ionophore

We test the proposed circuit analogy and applicability of the BFM speed as the voltmeter by applying a known membrane stress. We choose a cell signaling molecule indole that at millimolar concentrations forms a dimer and acts as an ionophore (19). Ionophores are molecules that carry ions across the lipid bilayer, thus we expect the membrane resistance to decrease (ion conductance increases) when indole is present in the medium. Furthermore, we expect to recover previously demonstrated parabolic dependence of membrane conductance on indole concentration (19).

Fig. 2A shows examples of individual motor speed recordings prior, during and post treatment with a given concentration of indole. Motor speed drops immediately with the addition of indole, and stays at approximately the same level until indole is removed, at which point it recovers to the initial level. The speed change caused by indole is faster than 10 ms (our experimental resolution), confirming the estimate of membrane RC constant, and justifying the assumption that the current through the capacitance in Fig. 1A circuit is negligible. Indole

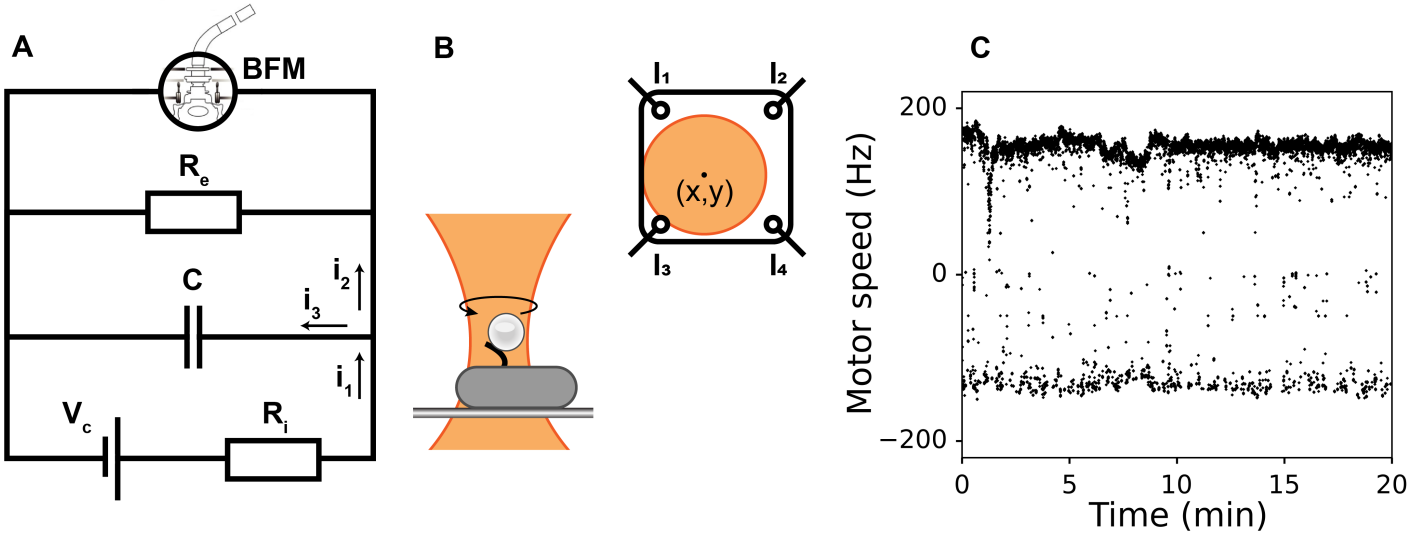

Figure 1. (**A**) Electric circuit equivalent of an *E. coli* cell. Oxidative (or substrate-level) phosphorylation is shown as a battery V_c with an internal resistance R_i, the membrane with capacitance C and resistance R_e, and i_1 to i_3 are the currents. Bacterial flagellar motor (BFM) is shown as a "voltmeter" that measures membrane potential, V_m. (**B**) Schematic of the "bead-assay" and back-focal-plane interferometry. A cell is attached to a cover glass with a truncated flagellar filament made "sticky" to polystyrene beads. The bead is brought into a heavily attenuated optical trap and its position measured with position sensitive detector. I_1 to I_4 indicate currents read by the position sensitive detector at four different locations (see *Materials and Methods*). (**C**) An example of raw motor speed trace recorded with back-focal-plane interferometry. Positive frequencies correspond to counter-clockwise and negative to the clockwise rotation of the flagellar motor (27). In the subsequent figures we show absolute values of the rotational speeds.

solution used for the treatment contains low percentage of ethanol (up to 0.25%). SI Fig. 3 shows that traces of ethanol do not significantly affect the motor speed if indole is not present.

To confirm the dependence of the membrane resistance on indole we find the relative change in motor speed at a given stress concentration. Fig. 2B shows the mean speed traces for different indole concentrations (see *Materials and Methods* for mean speed calculation) and in Fig. 2C we plot the probability densities of preshock and shock speeds. From the Gaussian fits to preshock and shock speed distributions we obtain mean shock speeds for a given indole concentration, and plot them normalised to the preshock speed, Fig. 2D. We fit the normalised speeds with hyperbolic or quadratic hyperbolic function (see *Materials and Methods*, both of which yield good quality fits with R^2 higher than 0.90). The concentrations of indole at which the quadratic dependence becomes particularly obvious in previous study, range between 2 to 5 mM (19), whereas we observe a significant effect in the 0-2.5 mM range. The difference can be explained by variations in electrochemical properties of cells, kept or grown in different media and to a different growth stage. Another possible reason is a residual accumulation of indole in a cell membrane, which has been reported in a wild type indole-producing cells grown to late exponential phase (39) (Chimerel *et al.* in their work used an indole non-producing strain (19)). However, BFM speed recovers to the same level after indole removal (Fig. 2). Thus, if there is a residual accumulation of indole it is kept constant during the experiments.

Butanol acts as an ionophore, changing membrane conductance linearly with concentration

To determine the mechanism of action of an unknown stress we choose butanol. Previous work indicates that butanol interacts with cell membrane and weakens it, but the exact mechanism of cell damage is unknown (40).

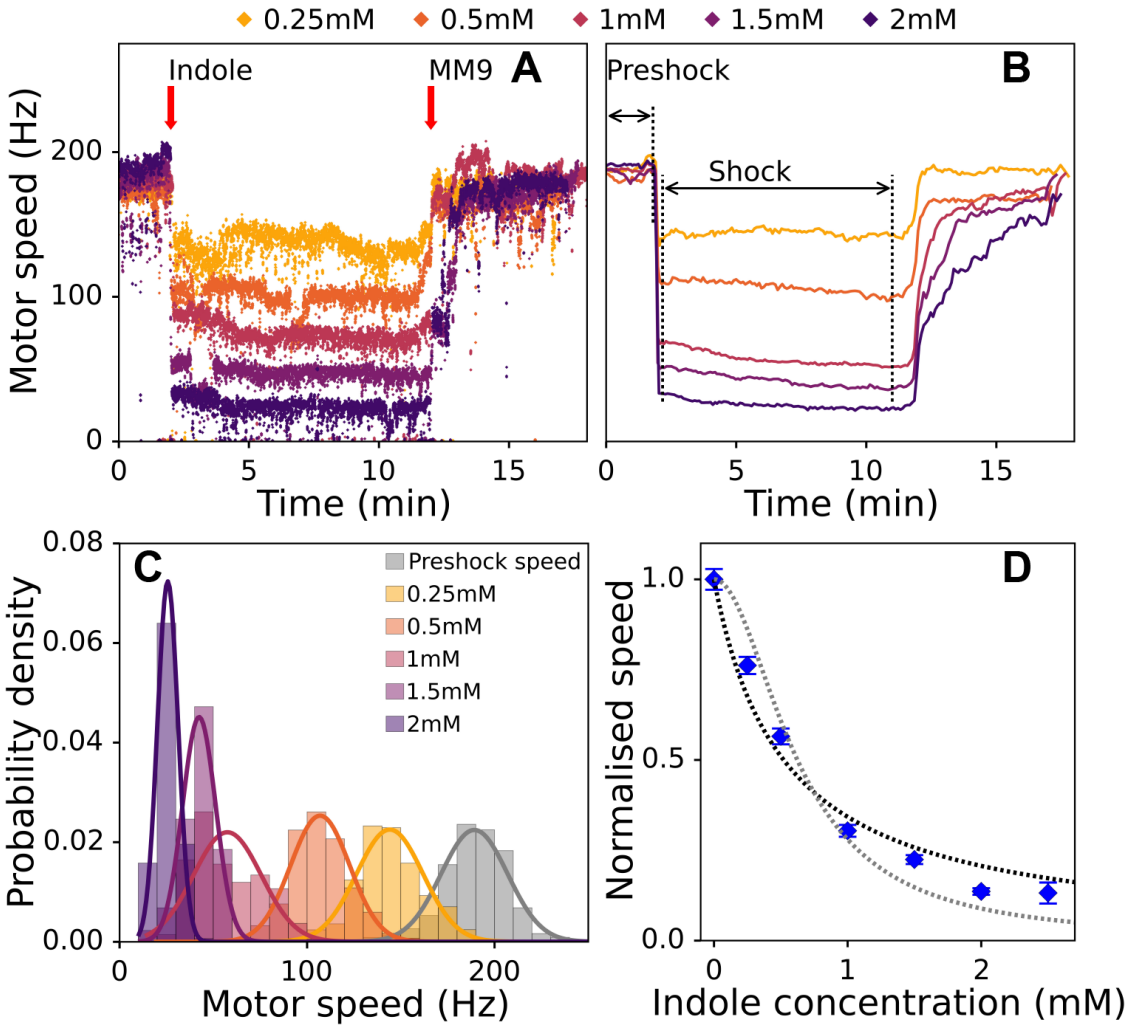

Figure 2. BFM speed drops rapidly and increasingly with increasing indole concentration (**A**) Examples of raw motor speed traces at 5 different indole concentrations. Indole is delivered into the tunnel-slide 2 min after the recording commences, and removed after 12 min. (**B**) Mean speeds of n⩾20 motor speeds for each indole concentration are shown against time. Each motor recording is performed on a different cell, thus the number of motors corresponds to the number of different individual cells. Preshock speed is calculated for time interval between 0 and 110 s (indicated in the figure). Shock speed is calculated from the 130 to 660 s of the motor recording. Preshock and shock intervals were chosen to exclude the duration of the flush. Standard errors are given, but not visible (for standard deviations see SI Fig. 7A). (**C**) Probability density of motor speeds for each indole concentration. Experimental data is fitted with a Gaussian probability density function. (**D**) Normalised BMF speeds plotted against indole concentration. Error bars represent standard error of the mean, and dotted lines show hyperbolic (black) and quadratic hyperbolic (grey) fit ($R^2 = 0.97$ and $R^2 = 0.95$ respectively).

We perform the BFM speed measurements in *E. coli* cells treated with butanol. The experimental protocol of butanol delivery is the same as for indole. Fig. 3A and 3B show examples of raw traces and mean speed traces prior, during and post butanol shock in MM9. Immediately upon butanol stress motor speed drops, and upon butanol removal it recovers to the initial value, Fig. 3A. Motor speed distributions at a given butanol concentrations remain narrow, and we fit them with Gaussian curves (Fig. 3C). Fig. 3D shows normalised motor speeds, calculated as mean values of the distributions given in Fig. 3C, and plotted against butanol concentration

for both MM9 media and PBS.

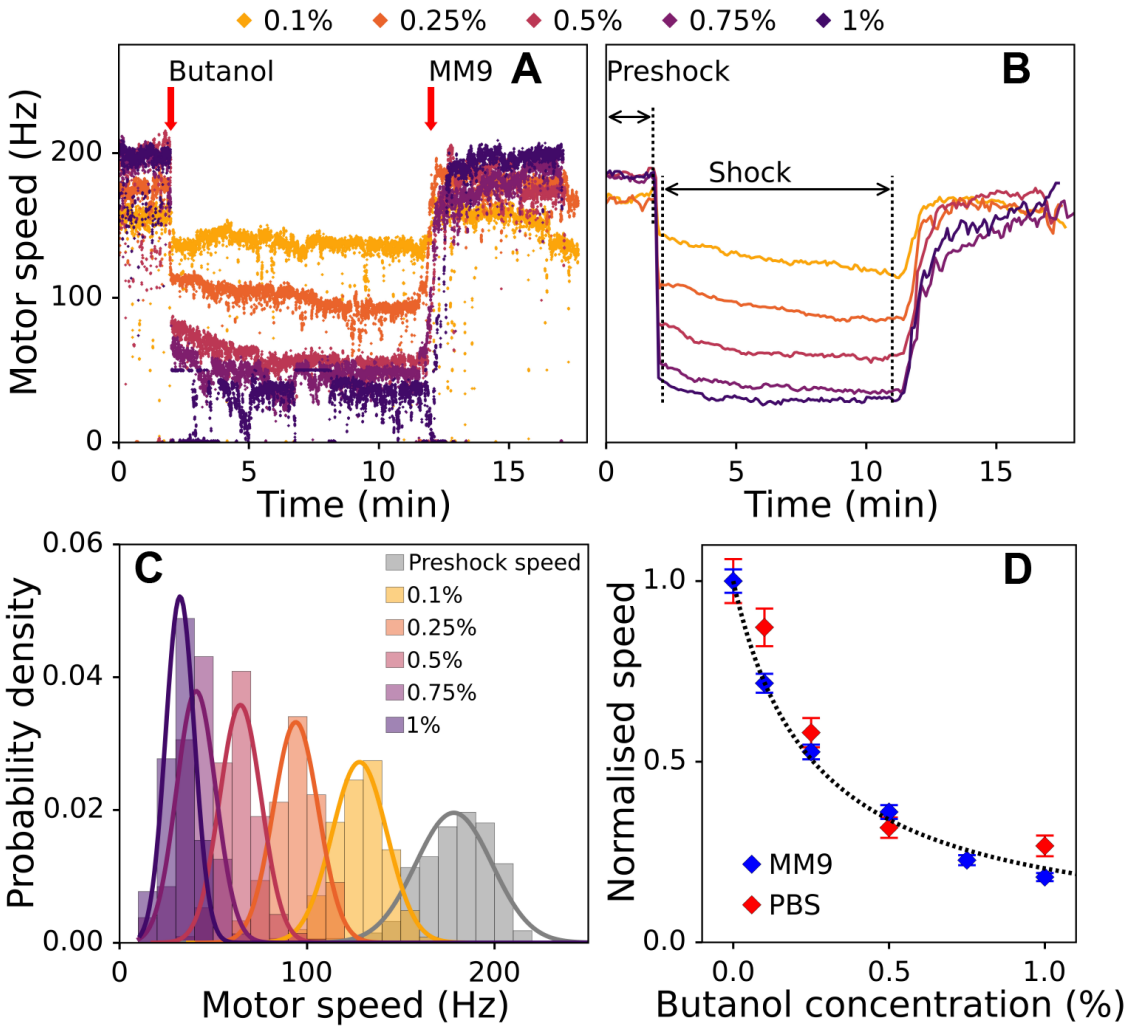

Figure 3. BFM speed drops sharply and reversibly after butanol treatment. (**A**) Examples of raw BFM speed traces for 5 different butanol concentrations. Butanol is delivered 2 min into the recording and removed after 12 min. (**B**) Mean speeds of n⩾20 cells per different butanol concentrations are plotted against time. Preshock and shock speeds are calculated in the 0 to 110 s, and 130 to 660 s time interval, respectively. Standard errors of the mean are given, but not visible. Standard deviations of the same traces are given in SI Fig. 7B. (**C**) Probability densities of shock speed for each butanol concentration and the preshock speed. (**D**) Shock speeds obtained from the distributions are normalised by the preshock speed and plotted against butanol concentration. Blue diamonds show cells in MM9 media and red diamonds cells in PBS. Error bars represent standard error of the mean. Hyperbolic fit is given as a black dotted line ($R^2 = 0.96$).

The relative speed drop observed in the presence of butanol is media independent, and alike that observed for indole. The finding suggesting that, on the time scale of our experiment, butanol cause non-permanent membrane damage and acts as an ionophore. The normalised motor speed dependence on butanol concentration is hyperbolic, and we obtain equation (3c) for membrane resistance:

$$R_e = \frac{R_{e,0}}{7.8 \cdot c_{but} + 1} \tag{4}$$

where c_{but} is a butanol concentration in percents (%) and 7.8 is a value of constant K obtained from the hyperbolic fit (see *Materials and Methods*). We observe the speed restoration after butanol removal even after multiple treatments of the same cell. SI Fig. 8 shows several consecutive butanol stresses each lasting 60 s (A) or 30 s (B), where after each treatment motor speed is fully restored.

Photodamage increases membrane conductance that scales with the light power

As an example of a complex stress we next choose to characterise light induced damage. While previous reports indicate that light causes wavelength dependent damage to bacterial cells (41; 42), they also suggest that the nature of damage is complex. Most likely the cause of the damage is formation of reactive oxygen species (ROS) (43; 44), which have been shown to perturb multiple components of the cell: DNA, RNA, proteins and lipids (45; 46). To apply light of a certain wavelength and intensity to bacterial cells we use a flow-cell (see *Materials and Methods*). During the light exposure cells are continuously supplied with fresh media at 10 μl/min flow rate. We apply the light of 395 nm and 475 nm wavelengths as the choice allows us to simultaneously measure internal pH of bacteria.

Fig. 4A shows example BFM speed traces during exposure to light of different effective powers (P_{eff}) delivered to the cells. P_{eff} is calculated as the total energy delivered divided by the total time the light is on (see *Materials and Methods*). Fig. 4A shows that BFM speed gradually decreases in time during exposure to light and that the decrease rate scales with the P_{eff}, also visible in Fig. 4B showing mean BFM speed traces for the same four effective powers.

To identify the functional dependence of the speed decrease rate on P_{eff} we fit individual normalised traces with the simple exponential function: $\omega/\omega_0 = e^{-\alpha t}$, with the single fitting parameter α. Mean of the fits with standard errors at corresponding four different powers are shown in Fig. 4C, and Fig. 4D shows fit coefficient α plotted against the light power for both MM9 medium and PBS. The effect of light on V_m is present in PBS and of same functional dependence, thus on the time scales of our experiment light affects primarily the membrane resistance, R_e. Together with the fact that the speed decrease rates stay the same at a given P_{eff}, the finding suggests that on the time scale of our experiment there is no active membrane repair. We further confirm this by measuring the motor speed after we expose the cells to light for shorter periods of time. SI Fig. 9 shows that when the illumination ceases after 5 or 15 min the (decreased) BFM speed remains the same with no visible recovery. We also check that light damage is not enhanced by the presence of the fluorescent protein (pHluorin) in the cytoplasm, SI Fig. 10.

Fig. 4D enables us to determine functional relationship between effective power and α, which increases as a logarithm of the normalised P_{eff}, i.e. $P_{eff,norm} = P_{eff}/(\mathrm{mW}\cdot\mathrm{cm}^{-2})$. Thus, for our initial exponential fit we obtain:

$$\omega = \omega_0 \cdot e^{-(a \ln P_{eff,norm} + b)t} \tag{5}$$

where a and b are wavelength specific parameters, a = 0.00064 s^{-1} and b = -0.00181 s^{-1} and equation (5) holds for $P_{eff} > P_{eff,0}$.

The minimum power required for the damage to occur is defined as $P_{eff,0} = e^{-\frac{b}{a}}$ mW/cm^2, and for 395 nm and 475 nm this is $\sim$ 17 mW/cm^2. Re-writing the equation (5) in terms of $P_{eff,0}$ we get:

$$\omega = \omega_0 \left(\frac{P_{eff,0}}{P_{eff}} \right)^{at} \tag{6}$$

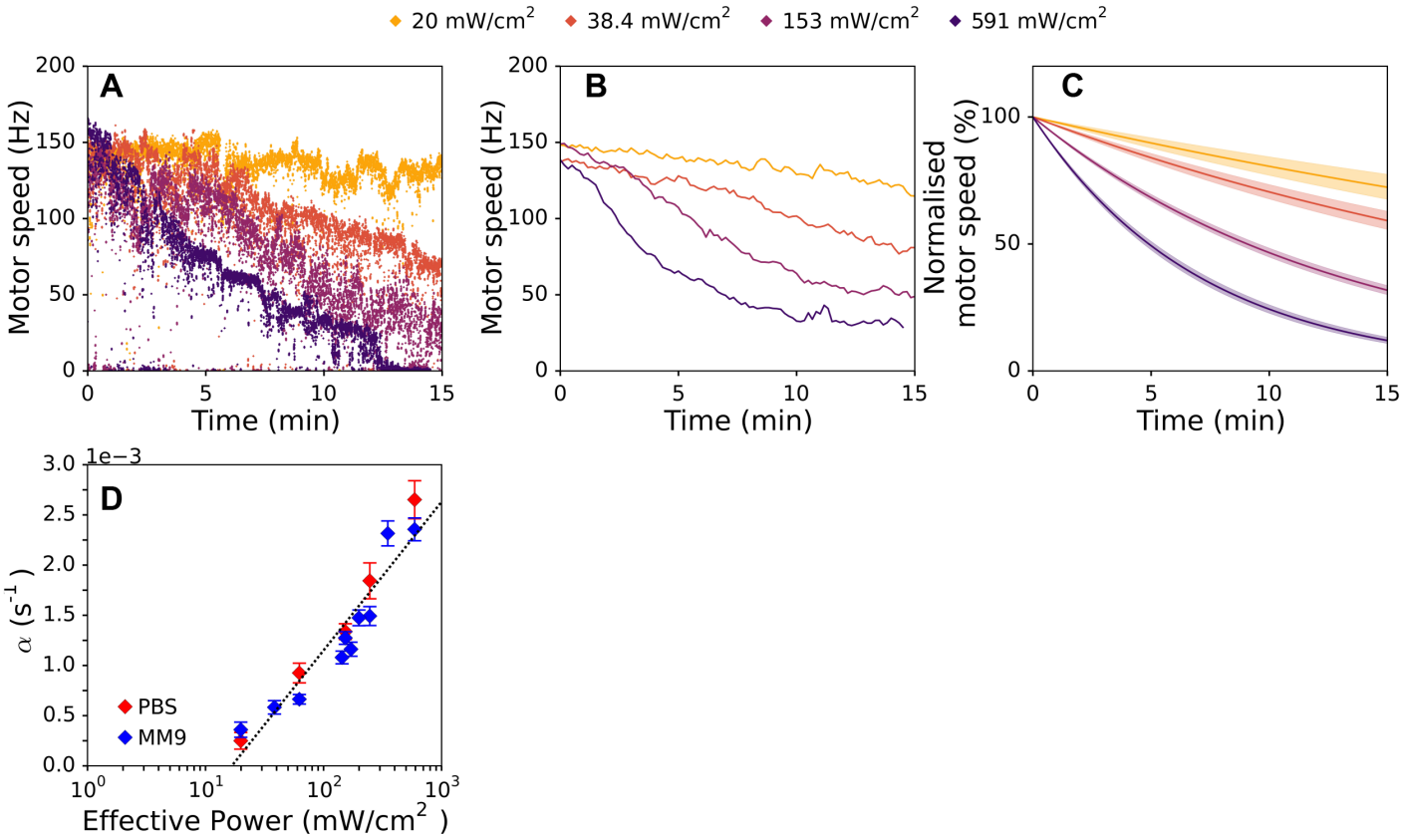

Figure 4. Rate of the motor speed decay increases with the light power. (**A**) Examples of raw traces at four different effective powers, P_{eff} = 20, 38.4, 153 or 591 mW/cm^2. (**B**) Mean BFM speed at different illumination powers (21 to 34 cells are recorded per condition). (**C**) Averaged exponential fits for different illumination powers with standard error. Each individual motor trace is fitted with an exponential function and the mean of fitting parameter α is calculated for each P_{eff}. (**D**) Exponential fit coefficient α is plotted against illumination power. Blue diamonds show cells in MM9 media and red diamonds cells in PBS. Error bars represent standard error and dotted line the logarithmic fit (R^2 = 0.906). The total number of cells in MM9 is 277 and in PBS 116.

Finally, applying (6) to equation (3c) we derive R_e functional dependence on the effective power:

$$R_e = \frac{R_{e,0}}{2\left(\frac{P_{eff}}{P_{eff,0}}\right)^{at} - 1}, \tag{7}$$

where a is the fit coefficient in Fig. 4D.

DISCUSSION

Arguably, one of the defining features of life is its ability to avoid thermodynamic equilibrium (death) by achieving a steady state supply of free energy. Chemiosmotic theory explained that the production of life's energy currency, the ATP molecule, proceeds via the generation of trans-membrane electrochemical potential. The ability to measure and control voltage and current across the cellular membrane with the patch-clamp technique had far reaching consequences for our understanding of cells such as neurones, where the electrical inputs govern signal transmission (36). In the cases of bacteria, and their small size, we are unable to gain the

same level of control over these parameters (47; 48), despite the fact that the ability to do so would open a range of currently inaccessible questions that are at the basis of bacterial free energy maintenance, and consequently, survival.

Here we demonstrate the use of BFM as a fast voltmeter, enabling quantitative, *in vivo* studies of electrochemical properties of the bacterial membrane. Alternative methods for measuring V_m in *E. coli* rely on fluorescent readout (49; 50; 51). However, Nernstian dyes (49; 50) sometimes fail to penetrate *E. coli's* membrane (52), can be a substrate for the outer membrane efflux system TolC (53) and in external conditions where they do equilibrate across the membrane, they do so on the time scales of minutes (52; 54). Voltage sensitive membrane proteins that can be used in *E. coli* require delivery of light of high power (51). BFM, on the other hand, is native to *E. coli* and expressed in a range of conditions (55). Speed measurements via back-focal-plane interferometry or fast cameras do not rely on fluorescent illumination and offer high time resolution (up to 0.5 ms (56)).

We choose to work with cells grown into late exponential phase in LB, as this has been shown to maximise the number of motors expressed per cell (26). However, our methodology is applicable across a range of growth conditions. Cremer *et al.* demonstrate that cells in steady-state (exponential) growth express motors in both rich and poor media (55). To obtain steady-state growth, cells from an overnight (stationary) culture need to divide sufficient number of times before running out of nutrients, which is easiest achieved by ample dilutions into the fresh media. We expect that the cells grown in different media will have different electrochemical properties, which can be measured with our approach in the future.

In this work we choose conditions that satisfy $\Delta pH \approx 0$, and thus V_m is the only contribution to the PMF. However, BFM speed measurements can be extended to conditions where ΔpH contribution to the PMF is not negligible, V_m in this case will be calculated from equation (1). Extending the use of BFM as the voltmeter for long term measurements (into hours and days) is possible. We note that on longer time scales motor can be actively slowed down via YcgR protein (34; 57), and such long term measurements would likely require YcgR deletion background. We also note that we have assumed only one of the components of the circuit is affected by the stress, as most stresses predominantly act on one of the circuit components immediately post application. To apply the approach to the stresses that change two or more components at a time further assumptions regarding the stress function will be required to introduce additional equations into the circuit model.

We base the use of BFM as the cell's voltmeter on the proportionality between motor speed and PMF, measured first more than 20 years ago (17; 18). Recent experiments show that BFM also exhibits mechanosensing (58; 59), where stator unit incorporation depends on the motor torque. These recent findings indicate an intriguing control mechanism, where mechanosensing and the ion flux combined result in the characteristic proportional relationship between the BFM speed and PMF. It will be interesting to fully ascertain the exact molecular mechanism behind the PMF-motor speed relationship, and we think the ability to fine-control the PMF loss can contribute to that understanding.

Using the electric circuit analogy for the membrane fluxes, and BFM as the cell's "voltmeter" we demonstrate the effect of three different stresses on the cell's membrane conductance. For the known stress, indole, we confirm it acts as an ionophore. For the first unknown stress we applied, butanol, we show its presence decreases membrane resistance, inversely proportional to the butanol concentration. Thus, we conclude that, in the concentration range we tested and on the 15 min time scale, butanol behaves as an ionophore in a manner similar to indole or CCCP (19). With analysis alike we presented, butanol action can be characterised further, e. g. defining the minimum concentration and incubation time required for the effect to become irreversible. For our last stress, light of short wavelengths, we show that it affects membrane resistance and functionally describe the damage in relation to time and P_{eff}. Light-induced changes in membrane permeability have been reported in artificial planar lipid bilayer systems and liposomes in the presence of photosensitisers (60; 61; 62; 63). The most likely cause of such changes is ROS induced chain-reaction lipid peroxidation (64; 65; 66; 67; 68). Presence of peroxidised lipids can change bilayer physical and electrical properties (69; 70; 71), e.g. it has been

suggested that it induces formation of hydrophobic pre-pores and their later transformation into hydrophilic pores permeable to ions (62; 63). Based on the previous work, and our real time, *in vivo* measurements we propose the following model for the complex nature of the light-induced membrane damage. Exposure to light causes the formation of ROS that induce lipid peroxidation, and thus alter the electric properties of the membrane. In particular, its permeability to ions due to the formation of hydrophilic pores. In contrast to the ionophores that carry ions across the membrane without causing membrane damage, the drop in V_m we observe under light proceeds as a result of slower, multi-step formation of lipid pores that require active repair to be mitigated. Therefore, we do not see any fast recovery after illumination ceases (SI Fig. 9).

Living cells have built-in mechanisms of coping with oxidative stress, for example SoxRS/OxyR regulons containing multiple antioxidant-encoding genes, such as *sodA* (manganese superoxide dismutase) or *katG* (hydroperoxidase I) (72; 71). The existence of defence mechanisms explains the occurrence of the minimum power required to cause the damage. Less power, even if it causes ROS formation, will not damage the cells that cope using internal protection enzymes. The value of the minimal damage-causing power we measured can indicate the abundance of internal protective resources available to the cell, as well as define the power range for fluorescence imaging that should be used to ensures no (unaccounted for) damage is inflicted to the cells by the exposure to light.

Future applications of our approach include, but are not limited to, studying other damage mechanisms and characterising unknown bacterial membrane properties, e.g. overal resistance in different growth conditions. Lastly, based on our measurements we suggest the use of light for delivery of small molecules, such as antimicrobial peptides or fluorescent dyes, which otherwise fail to penetrate *E. coli's* membrane (52).

Author Contributions

EK, CJL and TP designed research. EK performed research and analysed data. EK, CJL and TP interpreted results and wrote the paper.

Acknowledgements

We thank all the members of Pilizota and Lo laboratories, Zaki Leghtas, Jelena Baranovic, Bai Fan, Peter Swain, Ivan Maryshev, Ivan Erofeev, Calin Guet and Munehiro Assaly for useful discussions. EK was supported by the Global Research and Principal's Career Development PhD Scholarships. TP and CJL were supported by the Human Frontier Science Program Grant (RGP0041/2015), and CJL by the Ministry of Science and Technology, Republic of China (MOST-107-2112-M-008-025-MY3).

REFERENCES

[1] S. Keis, A. Stocker, P. Dimroth, and G. M. Cook, "Inhibition of ATP hydrolysis by thermoalkaliphilic F1F 0-ATP synthase is controlled by the C terminus of the ε subunit," *Journal of Bacteriology*, vol. 188, no. 11, pp. 3796–3804, 6 2006.

[2] L. Galvani, "De viribus electricitatis in motu musculari commentarius," *De Bononiensi Scientiarum et Artium Instituto atque Academia Commentarii, tomus septimus.*, pp. 363–418, 1791.

[3] R. M. Green, "A Translation of Luigi Galvani's De viribus electricitatis in motu musculari commentarius. Commentary on the Effect of Electricity on Muscular Motion," *Journal of the American Medical Association*, vol. 153, no. 10, p. 989, 11 1953.

[4] H. Fricke, "The electric capacity of cell suspension," *Physical Review*, vol. 21, pp. 708–709, 1923.

[5] P. Mitchell, "Coupling of phosphorylation to electron and hydrogen transfer by a chemi-osmotic type of mechanism," *Nature*, vol. 191, no. 4784, pp. 144–148, 7 1961.

[6] P. C. Nelson, *Biological Physics: Energy, Information, Life*. Freeman, W.H., 2003.

[7] B. J. Van Rotterdam, W. Crielaard, I. H. Van Stokkum, K. J. Hellingwerf, and H. V. Westerhoff, "Simplicity in complexity: The photosynthetic reaction center performs as a simple 0.2 V battery," *FEBS Letters*, vol. 510, no. 1-2, pp. 105–107, 1 2002.

[8] J. M. Walter, D. Greenfield, C. Bustamante, and J. Liphardt, "Light-powering Escherichia coli with proteorhodopsin." *Proceedings of the National Academy of Sciences of the United States of America*, vol. 104, no. 7, pp. 2408–12, 2 2007.

[9] J. L. Slonczewski, B. P. Rosen, J. R. Alger, and R. M. Macnab, "pH homeostasis in Escherichia coli: measurement by 31P nuclear magnetic resonance of methylphosphonate and phosphate." *Proceedings of the National Academy of Sciences of the United States of America*, vol. 78, no. 10, pp. 6271–6275, 1981.

[10] D. Zilberstein, V. Agmon, S. Schuldiner, and E. Padan, "Escherichia coli intracellular pH, membrane potential, and cell growth," *Journal of Bacteriology*, vol. 158, no. 1, pp. 246–252, 1984.

[11] J. C. Wilks and J. L. Slonczewski, "pH of the cytoplasm and periplasm of Escherichia coli: Rapid measurement by green fluorescent protein fluorimetry," *Journal of Bacteriology*, vol. 189, no. 15, pp. 5601–5607, 8 2007.

[12] T. Noumi, M. Maeda, and M. Futai, "Mode of inhibition of sodium azide on H+-ATPase of Escherichia coli," *FEBS Letters*, vol. 213, no. 2, pp. 381–384, 3 1987.

[13] Y. Sowa and R. M. Berry, "Bacterial flagellar motor," *Quarterly Reviews of Biophysics*, vol. 41, no. 2, pp. 103–132, 2008.

[14] M. D. Manson, P. M. Tedesco, and H. C. Berg, "Energetics of flagellar rotation in bacteria," *Journal of Molecular Biology*, vol. 138, no. 3, pp. 541–561, 4 1980.

[15] S. Matsuura, J. i. Shioi, and Y. Imae, "Motility in Bacillus subtilis driven by an artificial protonmotive force," *FEBS Letters*, vol. 82, no. 2, pp. 187–190, 10 1977.

[16] M. Meister, G. Lowe, and H. C. Berg, "The proton flux through the bacterial flagellar motor," *Cell*, vol. 49, no. 5, pp. 643–650, 1987.

[17] D. C. Fung and H. C. Berg, "Powering the flagellar motor of Escherichia coli with an external voltage source," *Nature*, vol. 375, no. 6534, pp. 809–812, 1995.

[18] C. V. Gabel and H. C. Berg, "The speed of the flagellar rotary motor of Escherichia coli varies linearly with protonmotive force." *Proceedings of the National Academy of Sciences of the United States of America*, vol. 100, no. 15, pp. 8748–8751, 7 2003.

[19] C. Chimerel, C. M. Field, S. Piñero-Fernandez, U. F. Keyser, and D. K. Summers, "Indole prevents Escherichia coli cell division by modulating membrane potential," *Biochimica et Biophysica Acta - Biomembranes*, vol. 1818, no. 7, pp. 1590–1594, 7 2012.

[20] C. S. Barker, B. M. Prüß, and P. Matsumura, "Increased motility of Escherichia coli by insertion sequence element integration into the regulatory region of the flhD operon," *Journal of Bacteriology*, vol. 186, no. 22, pp. 7529–7537, 11 2004.

[21] G. Kuwajima, "Construction of a minimum-size functional flagellin of Escherichia coli," *Journal of Bacteriology*, vol. 170, no. 7, pp. 3305–3309, 7 1988.

[22] G. Miesenböck, D. A. De Angelis, and J. E. Rothman, "Visualizing secretion and synaptic transmission with pH-sensitive green fluorescent proteins," *Nature*, vol. 394, no. 6689, pp. 192–195, 1998.

[23] Y. V. Morimoto, S. Kojima, K. Namba, and T. Minamino, "M153R mutation in a pH-sensitive green fluorescent protein stabilizes its fusion proteins," *PLoS ONE*, vol. 6, no. 5, p. e19598, 2011.

[24] T. Pilizota and J. W. Shaevitz, "Fast, multiphase volume adaptation to hyperosmotic shock by Escherichia coli." *PLoS ONE*, vol. 7, no. 4, p. e35205, 4 2012.

[25] A. J. Link and D. Phillips, "Methods for generating precise deletions and insertions in the genome of wild-type Escherichia coli : application to open reading frame characterization," *Journal of Bacteriology*, vol. 179, no. 20, pp. 6228–6237, 1997.

[26] C. D. Amsler, M. Cho, and P. Matsumura, "Multiple factors underlying the maximum motility of Escherichia coli as cultures enter post-exponential growth," *Journal of Bacteriology*, vol. 175, no. 19, pp. 6238–6244, 1993.

[27] F. Bai, R. W. Branch, D. V. Nicolau, T. Pilizota, B. C. Steel, P. K. Maini, and R. M. Berry, "Conformational spread as a mechanism for cooperativity in the bacterial flagellar switch," *Science*, vol. 327, no. 5966, pp. 685–689, 2 2010.

[28] J. Rosko, V. Martinez, W. Poon, and T. Pilizota, "Osmotaxis in Escherichia coli through changes in motor speed," *Proceedings of the National Academy of Sciences of the United States of America*, vol. 114, no. 38, pp. E7969–E7976, 2017.

[29] Y. K. Wang, E. Krasnopeeva, S.-Y. Lin, F. Bai, T. Pilizota, and C.-J. Lo, "Comparison of Escherichia coli surface attachment methods for in vivo single-cell microscopy," *In preparation*, 2019.

[30] W. Denk and W. W. Webb, "Optical measurement of picometer displacements of transparent microscopic objects." *Applied optics*, vol. 29, no. 16, pp. 2382–2391, 6 1990.

[31] K. Svoboda, C. F. Schmidt, B. J. Schnapp, and S. M. Block, "Direct observation of kinesin stepping by optical trapping interferometry," *Nature*, vol. 365, no. 6448, pp. 721–727, 10 1993.

[32] R. Buda, Y. Liu, J. Yang, S. Hegde, K. Stevenson, F. Bai, and T. Pilizota, "Dynamics of Escherichia coli 's passive response to a sudden decrease in external osmolarity," *Proceedings of the National Academy of Sciences of the United States of America*, vol. 113, no. 40, pp. E5838–E5846, 10 2016.

[33] T. Nyström and N. Gustavsson, "Maintenance energy requirement: What is required for stasis survival of Escherichia coli?" *Biochimica et Biophysica Acta - Bioenergetics*, vol. 1365, no. 1-2, pp. 225–231, 1998.

[34] A. Boehm, M. Kaiser, H. Li, C. Spangler, C. A. Kasper, M. Ackermann, V. Kaever, V. Sourjik, V. Roth, and U. Jenal, "Second Messenger-Mediated Adjustment of Bacterial Swimming Velocity," *Cell*, vol. 141, no. 1, pp. 107–116, 4 2010.

[35] H. Fricke, H. P. Schwan, K. Li, and V. Bryson, "A dielectric study of the low-conductance surface membrane in E. coli," *Nature*, vol. 177, no. 4499, pp. 134–135, 1 1956.

[36] A. L. Hodgkin, A. F. Huxley, and B. Katz, "Measurement of current-voltage relations in the membrane of the giant axon of Loligo," *The Journal of Physiology*, vol. 116, no. 4, pp. 424–448, 1952.

[37] V. Miyamoto and T. Thompson, "Some electrical properties of lipid bilayer membranes," *Journal of Colloid and Interface Science*, vol. 25, no. 1, pp. 16–25, 9 1967.

[38] Q. H. Tran and G. Unden, "Changes in the proton potential and the cellular energetics of Escherichia coli during growth by aerobic and anaerobic respiration or by fermentation," *European Journal of Biochemistry*, vol. 251, no. 1-2, pp. 538–543, 1 1998.

[39] H. Gaimster, J. Cama, S. Hernández-Ainsa, U. F. Keyser, and D. K. Summers, "The indole pulse: A new perspective on indole signalling in Escherichia coli," *PLoS ONE*, vol. 9, no. 4, p. e93168, 4 2014.

[40] E. Fletcher, T. Pilizota, P. R. Davies, A. McVey, and C. E. French, "Characterization of the effects of n-butanol on the cell envelope of E. coli," *Applied Microbiology and Biotechnology*, vol. 100, no. 22, pp. 9653–9659, 11 2016.

[41] A. Ashkin, J. M. Dziedzic, and T. Yamane, "Optical trapping and manipulation of single cells using infrared laser beams," *Nature*, vol. 330, no. 6150, pp. 769–771, 12 1987.

[42] K. C. Neuman, E. H. Chadd, G. F. Liou, K. Bergman, and S. M. Block, "Characterization of photodamage to Escherichia coli in optical traps," *Biophysical Journal*, vol. 77, no. 5, pp. 2856–2863, 11 1999.

[43] T. L. de Jager, A. E. Cockrell, and S. S. Du Plessis, "Ultraviolet Light Induced Generation of Reactive Oxygen Species," in *Ultraviolet Light in Human Health, Diseases and Environment. Advances in Experimental Medicine and Biology*, S. Ahmad, Ed. Springer, Cham, 2017, pp. 15–23.

[44] D. B. Lockwood, J. C. Wataha, J. B. Lewis, W. Y. Tseng, R. L. W. Messer, and S. D. Hsu, "Blue light generates reactive oxygen species (ROS) differentially in tumor vs. normal epithelial cells," *Dental*

Materials, vol. 21, no. 7, pp. 683–688, 7 2005.

[45] E. Cabiscol, J. Tamarit, and J. Ros, "Oxidative stress in bacteria and protein damage by reactive oxygen species," *International Microbiology*, vol. 3, no. 1, pp. 3–8, 3 2000.

[46] X. Zhao and K. Drlica, "Reactive oxygen species and the bacterial response to lethal stress," *Current Opinion in Microbiology*, vol. 21, pp. 1–6, 10 2014.

[47] H. J. Ruthe and J. Adler, "Fusion of bacterial spheroplasts by electric fields," *Biochimica et Biophysica Acta - Biomembranes*, vol. 819, no. 1, pp. 105–113, 9 1985.

[48] B. Martinac, M. Buechner, A. H. Delcour, J. Adler, and C. Kung, "Pressure-sensitive ion channel in Escherichia coli." *Proceedings of the National Academy of Sciences of the United States of America*, vol. 84, no. 8, pp. 2297–2301, 4 1987.

[49] B. Ehrenberg, V. Montana, M. D. Wei, J. P. Wuskell, and L. M. Loew, "Membrane potential can be determined in individual cells from the nernstian distribution of cationic dyes," *Biophysical Journal*, vol. 53, no. 5, pp. 785–794, 1988.

[50] A. Prindle, J. Liu, M. Asally, S. Ly, J. Garcia-Ojalvo, and G. M. Süel, "Ion channels enable electrical communication in bacterial communities," *Nature*, vol. 527, no. 7576, pp. 59–63, 11 2015.

[51] J. M. Kralj, D. R. Hochbaum, A. D. Douglass, and A. E. Cohen, "Electrical spiking in Escherichia coli probed with a fluorescent voltage-indicating protein," *Science*, vol. 333, no. 6040, pp. 345–348, 7 2011.

[52] C. J. Lo, M. C. Leake, T. Pilizota, and R. M. Berry, "Nonequivalence of membrane voltage and ion-gradient as driving forces for the bacterial flagellar motor at low load," *Biophysical Journal*, vol. 93, no. 1, pp. 294–302, 7 2007.

[53] L. Mancini, T. Tian, G. Terradot, Y. Pu, F. Bai, and T. Pilizota, "Escherichia coli's physiology can turn membrane voltage dyes into actuators," *In preparation*, 2019.

[54] J. D. te Winkel, D. A. Gray, K. H. Seistrup, L. W. Hamoen, and H. Strahl, "Analysis of Antimicrobial-Triggered Membrane Depolarization Using Voltage Sensitive Dyes," *Frontiers in Cell and Developmental Biology*, vol. 4, p. 29, 2016.

[55] J. Cremer, T. Honda, Y. Tang, J. Ng, M. Vergassola, and T. Hwa, "Growth and migration of chemotactic bacterial populations in nutrient-replete environments," *Nature, in revision*, 2019.

[56] T. Pilizota, T. Bilyard, F. Bai, M. Futai, H. Hosokawa, and R. M. Berry, "A programmable optical angle clamp for rotary molecular motors," *Biophysical Journal*, vol. 93, no. 1, pp. 264–275, 7 2007.

[57] K. Paul, V. Nieto, W. C. Carlquist, D. F. Blair, and R. M. Harshey, "The c-di-GMP Binding Protein YcgR Controls Flagellar Motor Direction and Speed to Affect Chemotaxis by a "Backstop Brake" Mechanism," *Molecular Cell*, vol. 38, no. 1, pp. 128–139, 4 2010.

[58] P. P. Lele, B. G. Hosu, and H. C. Berg, "Dynamics of mechanosensing in the bacterial flagellar motor," *Proceedings of the National Academy of Sciences of the United States of America*, vol. 110, no. 29, pp. 11 839–11 844, 2013.

[59] M. J. Tipping, N. J. Delalez, R. Lim, R. M. Berry, and J. P. Armitage, "Load-dependent assembly of the bacterial flagellar motor," *mBio*, vol. 4, no. 4, 2013.

[60] D. G. McRae, E. Yamamoto, and G. H. Towers, "The mode of action of polyacetylene and thiophene photosensitizers on liposome permeability to glucose," *Biochimica et Biophysica Acta - Biomembranes*, vol. 821, no. 3, pp. 488–496, 12 1985.

[61] A. Pashkovskaya, E. Kotova, Y. Zorlu, F. Dumoulin, V. Ahsen, I. Agapov, and Y. Antonenko, "Light-triggered liposomal release: Membrane permeabilization by photodynamic action," *Langmuir*, vol. 26, no. 8, pp. 5725–5733, 2010.

[62] E. A. Kotova, A. V. Kuzevanov, A. A. Pashkovskaya, and Y. N. Antonenko, "Selective permeabilization of lipid membranes by photodynamic action via formation of hydrophobic defects or pre-pores," *Biochimica et Biophysica Acta - Biomembranes*, vol. 1808, no. 9, pp. 2252–2257, 2011.

[63] J. Wong-Ekkabut, Z. Xu, W. Triampo, I. M. Tang, D. P. Tieleman, and L. Monticelli, "Effect of lipid peroxidation on the properties of lipid bilayers: A molecular dynamics study," *Biophysical Journal*, vol. 93, no. 12, pp. 4225–4236, 12 2007.

[64] A. W. Girotti, "Mechanisms of lipid peroxidation," *Journal of Free Radicals in Biology and Medicine*, vol. 1, no. 2, pp. 87–95, 1 1985.

[65] ——, "Photodynamic lipid peroxidation in biological systems." *Photochemistry and photobiology*, vol. 51, no. 4, pp. 497–509, 4 1990.

[66] B. Halliwell, S. Chirico, M. A. Crawford, K. S. Bjerve, and K. F. Gey, "Lipid peroxidation: Its mechanism, measurement, and significance," *American Journal of Clinical Nutrition*, vol. 57, no. 5 SUPPL., pp. 715S–725S, 5 1993.

[67] D. E. Heck, A. M. Vetrano, T. M. Mariano, and J. D. Laskin, "UVB light stimulates production of reactive oxygen species: Unexpected role for catalase," *Journal of Biological Chemistry*, vol. 278, no. 25, pp. 22 432–22 436, 6 2003.

[68] R. Lavi, A. Shainberg, V. Shneyvays, E. Hochauser, A. Isaac, T. Zinman, H. Friedmann, and R. Lubart, "Detailed analysis of reactive oxygen species induced by visible light in various cell types," *Lasers in Surgery and Medicine*, vol. 42, no. 6, pp. 473–480, 7 2010.

[69] G. E. Dobretsov, T. A. Borschevskaya, V. A. Petrov, and Y. A. Y. A. Vladimirov, "The increase of phospholipid bilayer rigidity after lipid peroxidation." *FEBS Letters*, vol. 84, no. 1, pp. 125–8, 12 1977.

[70] C. Richter, "Biophysical consequences of lipid peroxidation in membranes," *Chemistry and Physics of Lipids*, vol. 44, no. 2-4, pp. 175–189, 7 1987.

[71] E. Birben, U. Murat, S. Md, C. Sackesen, S. Erzurum, and O. Kalayci, "Oxidative Stress and Antioxidant Defense," *World Allergy Organization Journal*, vol. 5, no. 1, pp. 9–19, 1 2012.

[72] G. Storz and J. A. Imlayt, "Oxidative stress," *Current Opinion in Microbiology*, vol. 2, no. 2, pp. 188–194, 1999.

[73] C. Merlin, S. Mcateer, and M. Masters, "Tools for Characterization of Escherichia coli Genes of Unknown Function," *Journal of Bacteriology*, vol. 184, no. 16, pp. 4573–4581, 2002.

[74] K. A. Martinez, R. D. Kitko, J. P. Mershon, H. E. Adcox, K. A. Malek, M. B. Berkmen, and J. L. Slonczewski, "Cytoplasmic pH response to acid stress in individual cells of Escherichia coli and Bacillus subtilis observed by fluorescence ratio imaging microscopy," *Applied and Environmental Microbiology*, vol. 78, no. 10, pp. 3706–3714, 5 2012.

[75] M. Urh, D. Simpson, and K. Zhao, "Affinity Chromatography. General Methods," in *Methods in Enzymology*. Academic Press, 1 2009, vol. 463, no. C, ch. 26, pp. 417–438.

[76] N. Otsu, "A Threshold Selection Method from Gray-Level Histograms," *IEEE Transactions on Systems, Man, and Cybernetics*, vol. 9, no. 1, pp. 62–66, 1 1979.

[77] H. C. Berg and L. Turner, "Torque generated by the flagellar motor of Escherichia coli," *Biophysical Journal*, vol. 65, no. 5, pp. 2201–16, 11 1993.

[78] J. Rosko, "Osmotaxis in Escherichia coli," Ph.D. dissertation, The Edinburgh University, 2017.